Applied Thermal Engineering 260 (2025) 124918

Contents lists available at ScienceDirect

Applied Thermal Engineering

journal homepage: www.elsevier.com/locate/apthermeng

Research Paper

Porous mesh manifold for enhanced boiling performance

Roman Giglio [a,1], Muhammad R. Shattique [b,1], Ercan M. Dede [c], Sreekant Narumanchi [d], Mehdi Asheghi [e], Kenneth E. Goodson [e], James W. Palko [a,*]

[a] Department of Mechanical Engineering, University of California, Merced, CA, USA
[b] Materials and Biomaterials Science and Engineering Graduate Program, University of California, Merced, CA, USA
[c] Electronics Research Department Toyota Research Institute of North America, Ann Arbor, MI, USA
[d] National Renewable Energy Laboratory, Golden, CO, USA
[e] Department of Mechanical Engineering, Stanford University, Stanford, CA, USA

ARTICLE INFO

Keywords:
Boiling Enhancement
Critical Heat Flux
Electronics Cooling
Heat Transfer Coefficient
Porous Structures

ABSTRACT

High-performance electronics are continuously demanding cooling of higher heat fluxes. Phase-change cooling, including pool boiling, is a useful approach to address this challenge; however, competition between liquid and vapor flows generally limit the heat fluxes that can be dissipated. A range of strategies to control these flows have been investigated previously, including capillary guides. Here a manifold structure formed from a metallic mesh is investigated to control the disposition of liquid and vapor phases above a pool fed boiling surface enhanced with porous structures. Copper mesh forms defined liquid flow paths, using capillary action to guide and distribute liquid evenly over the heated surface, along with open channels to facilitate vapor escape. The mesh provides a novel structure for liquid guidance that imposes low resistance to liquid flow while occluding a minimal area of heated surface underneath. The manifold performance is characterized in boiling fed by a pool of water above a laser-textured aluminum nitride heat dissipation surface with pin–fin structures having heights of 110 μm and spacing of 30 μm with a heated area of 5 mm x 5 mm. A maximum heat flux of 490 W/cm^2 is reached with the manifold in the pool fed configuration, representing an increase of more than 65% over the porous pin fin surface alone. The maximum stable superheat observed for the manifold of 36 K is 14 K higher than that for the porous surface without the manifold. The factors limiting performance of the manifold are analyzed. High superheat is attributed to partial flooding of the boiling surface as suggested by the reduction in superheat using external suction. Similar systems and structures for enhanced two-phase cooling are compared.

1. Introduction

Thermal management is an important element in many advancing technologies. For example, power electronics have a constantly evolving need for removal of larger heat loads with lower thermal resistance.[1] Electric vehicles, renewable energy converters, radars, 3D-integrated microelectronics, and laser diodes are a few prominent examples of power electronic applications with severe thermal management constraints.[2–5] Various advanced applications target performance requiring dissipation of heat fluxes of 1 kW/cm^2 and beyond. Current approaches to cooling high heat loads primarily focus on single-phase liquid cooling, but phase-change liquid/vapor cooling offers potential for dissipation of larger heat fluxes with smaller thermal resistance.[6] The maximum heat flux that can be dissipated, or "critical heat flux" (CHF), is thus a key metric of performance for two-phase cooling approaches.

Phase-change cooling takes a variety of forms including pool boiling, flow boiling, and capillary- fed evaporation, but in all cases, the limits to dissipated heat flux are associated with the ability to deliver liquid to the phase-change surface. The flow of liquid is strongly influenced, in turn, by the presence of the emanating vapor. Improving device CHF requires control of the multiphase liquid/vapor flow.[7] Pool boiling from a flat, unmodified, hydrophilic surface in water provides a critical heat flux of ~ 115 W/cm^2 and a corresponding heat transfer coefficient of ~ 7.0 W/(cm^2·K).[8] Liang and Mudawar reviewed models describing CHF in pool boiling.[9,10] Models invoking hydrodynamic stability of the liquid and vapor disposition above the heated surface, such as those related to the Zuber model[11], are successful in predicting behavior for smooth, wetting surfaces. However, it has also been clearly

* Corresponding author.
E-mail address: jpalko@ucmerced.edu (J.W. Palko).
[1] equal contribution.

https://doi.org/10.1016/j.applthermaleng.2024.124918
Received 2 July 2024; Received in revised form 13 October 2024; Accepted 10 November 2024
Available online 12 November 2024
1359-4311/© 2024 The Authors. Published by Elsevier Ltd. This is an open access article under the CC BY license (http://creativecommons.org/licenses/by/4.0/).

Nomenclature

Symbols

u	Flow velocity [m/s]
μ	Dynamic viscosity [Pa • s]
δ	Width [m]
h	Height [m]

Greek Symbols

Δp	Pressure gradient [Pa/m]

Abbreviations

HTC	Heat transfer coefficient
TCR	Temperature coefficient of resistance
CHF	Critical heat flux

demonstrated that surface properties play an important role in determining CHF performance. Kandlikar proposed a model accounting for the effect of liquid contact angle,[12] and Rahman, et al. correlated CHF with the wicking capability of textured surfaces.[13]

The introduction of roughness or porous surface structures to a cooling surface is an effective method for enhancing performance of phase-change cooling. The study of surface enhancements is extensive and covered in various reviews including those of Liang and Mudawar [14] and Mori and Utaka.[15] Modghadasi et al. used photolithography to make a range of wick sizes to compare wettability/ porosity to heat transfer coefficient. The highest HTC was attributed to the surface with the most nucleation sites and surface area.[16] Mehdikhani et al. compared different methods using electro-deposition to make boiling surfaces. A maximum heat flux of 112.4 W/cm^2 is reached using a high-surface-area copper surface.[17] Haji et al. considered injection flow rate, solution concentration and spray time of titanium dioxide hydrophilic nanoparticles in electrostatic deposition and identified optimal parameters for this process for increasing critical heat flux and heat transfer coefficient.[18] The impact of wick conductivity on heat transfer effectiveness is studied by Lv et al.[19]

Rahman, et al. proposed a model accounting for the wicking effect of a porous surface in pool boiling.[13] This model invokes a mechanism of capillary wicking from regions of the surface that are wetted to those that are dry, e.g., under a bubble or vapor column. This situation is somewhat analogous to that of a porous surface experiencing evaporation while fed from the edges by capillary wicking, such as in a heat pipe. The performance of such a wick is determined by the viscous resistance for flow of both liquid and vapor phases. The flow directions of these phases are perpendicular. A thicker wick leads to lower flow resistance for the liquid in the plane of the wick but additional resistance for the vapor flow normal to the plane. Zhang et al. presented a model for this competition for a porous wick operating in boiling with an unobstructed vapor path above and a reservoir of liquid to the side.[20] The ultimate heat flux that can be dissipated in this situation is limited by the vapor flow resistance, and the area over which this flux can be removed is determined by the liquid resistance. For given wick pore size, liquid and vapor permeabilities, and thickness, there is a maximum distance, designated the critical wicking length, over which the capillary pressure supported by the wick can supply adequate liquid for the cooled area operating at the heat flux imposed by vapor escape from the wick. Beyond this length, partial dry-out of the wick will occur and only a portion of the wick will function. This is closely associated with the "boiling limit" of heat pipes where the low relative liquid permeability of the partially vapor saturated wicks provides the limit for maximum dissipated heat.[21] For an inverse opal wick with 5.4 μm minimum feature size and thickness of approximately 30 μm, the critical wicking length is approximately 300 μm.[20]

The stability of liquid flow paths to the heated surface, in opposition to the flow of the vapor away from the surface, is key to determining CHF in pool boiling. Multiple strategies have been implemented to ensure liquid delivery reaches the boiling surface evenly and adequately. These approaches control the distribution of liquid and vapor near the boiling surface to minimize competition between the two flows. Liter and Kaviany investigated porous surface coatings with modulated surface topography which impose the spacing of liquid and vapor jets.[22] An enhancement in CHF of more than 3x over a plain surface was demonstrated, and detailed models for the interaction of the porous layer and pool hydrodynamics for this and related systems were presented. Additional applied methods include partially insulated surfaces, mixed wettability surfaces, and hierarchal porous structures as discussed below.

One method that has shown effectiveness in directing liquid and vapor transport in pool boiling is controlling the flow of heat through the boiling surface via modulation of substrate thermal conductivity. This approach creates high heat flux regions where vapor is generated and low flux regions allowing liquid return. By controlling the positions of the regions, the competition between liquid supply and vapor escape is reduced. Rahman et al. introduced low conductivity strips to portions of a copper surface, lowering the total effective area but enhancing overall performance.[23] Xin, et al. show that low conductivity areas limit the size of the vapor bubbles, contributing to greater boiling performance in solutions with surfactants.[24] Heidary, et al. investigated the optimal ratio of insulated channel width, depth and pitch.[25] The researchers find that the channel pitch influences bubble departure diameter and that the shallowest insulating channels show the highest performance. In an additional study, Heidary et al. show the effect of adding channels with and without insulation to a boiling surface. It is found that the partially insulated surface has greater performance than that of the surface with a greater active area.[26] A cross pattern of low conductivity material was investigated by Xie et al.[27] and compared to a uniform surface and a bi-conductive parallel surface. The cross pattern of low conductivity material performed better than baseline studies, especially when the edges of the surface were left unmodified.

Another related approach modulates surface wettability creating "biphilic" surfaces. Hydrophilic regions have high wettability with enhanced heat flux dissipation capability as discussed above. Hydrophobic surfaces promote early onset of nucleate boiling (ONB) reducing superheat associated with incipience of boiling and resulting in high heat transfer coefficients. Betz et al. introduced Teflon (AF400, Dupont) islands onto a surface with high wettability. The critical heat flux and heat transfer coefficient were increased 65 % and 100 %, respectively, when compared to a purely hydrophilic surface.[28] Haji et al. considered multiple biphilic surface configurations to find an optimum. Critical heat flux and heat transfer coefficient are increased by 130.2 % and 140 %, respectively, compared to a plain copper surface.[29] Shim, et al. created a superbiphilic (SBPI) surface to direct liquid entry and vapor escape comprising a superhydrophilic, silicon nanowire base with fluoro-octyltrichloro silane superhydrophobic dots. The authors find a non-dimensional liquid supply factor to guide design of surfaces.[30] Three-dimensional structures have also been studied to further separate wetting and vapor growth. Zhang et al. demonstrated that rectangular fins with hydrophilic bases and hydrophobic tips can reduce the ONB superheat to 1°C.[31]

Hierarchical wicking structures have also been used, applying capillary action to promote fluid flow across a boiling surface. Many researchers have created tailored porous structures to move liquid across the boiling area of a capillary-fed surface.[32–38] Commonly, larger feature size wicks help move liquid across the boiling surface to feed smaller-feature-size wicks. The larger feature sizes result in higher permeability that can sustain higher flow rates. The smaller feature size wicks draw liquid from the larger wick to sustain boiling. This combination suppresses dry-out by supplying working fluid directly to dry areas on the boiling surface. Critical heat flux generally occurs when

available capillary suction is unable to supply necessary liquid flow through the combined resistance. A benefit of capillary-driven bi-porous structures is simplicity in design and application. Sudhakar et al. demonstrated a two-level wick that provided separate flow paths for vapor and liquid and even supply of liquid to the heat transfer surface via distributed connections between the two levels. This system dissipated up to 485 W/cm^2 over an area of 1 cm^2.[38]

Hierarchical surface modifications have also been used to influence the liquid and vapor flows above the surface in pool boiling. Patsuzko et al. examined both perforated foil and wire mesh additions to micro-fins. The highest performing test case was with micro-fins covered by a mesh with an aperture of 0.32 mm.[39] A study using a femtosecond laser to make rose petal inspired wicking structures was performed by Long et al.[40] Both wicks and liquid flow channels were made to improve nucleate boiling and rewetting, respectively. The rose petal wicking structures reach a CHF and HTC of 239.4 W/cm^2 and 26.0 $W/(cm^2 \cdot K)$, respectively. Wu et al. demonstrated the applicability of a picosecond laser to make ultrathin heat transfer devices. A novel grooved-porous composite wick structure was made on 0.6 mm thick copper plate. A combination of micro and nano groves is made to improve wettability.[41] Sun et al. shows that the simple application of a copper mesh above a sintered particle surface helps working fluid rewet the surface.[42] Mori et al. showed that adding a porous, honeycomb plate over a boiling surface can dramatically increase the critical heat flux,[43–45] achieving a CHF of 320 W/cm^2 in a water based TiO_2 nanofluid.[46] The authors propose a model for CHF for the system determined by the balance of the capillary pressure supplied by the porous honeycomb plate and the total pressure drop through the system including the viscous liquid and vapor losses and acceleration pressure.

The investigations discussed above show the potential to enhance CHF in pool boiling via combinations of porous surface enhancements with structures to direct liquid and vapor flow above the surface. Theoretically, carefully designed guiding structures evenly distributing liquid over porous surfaces should be able to dissipate heat fluxes nearing the intrinsic local limit of the porous surface itself, imposed by vapor escape and exceeding 1 kW/cm^2 for small wicking distances (e.g. several hundred microns).[20] The performance of current systems is well below these limits, and a number of outstanding questions remain regarding the design of these systems. As shown by Mori, et al.,[43] the resistance for liquid supply from the pool must be minimized while still maintaining adequate control of the distribution of liquid and vapor and not blocking vapor escape from a large portion of the heated surface. Preferred or optimal forms of a capillary structure to guide liquid have not been determined. Likewise, while there has been significant investigation of the influence of surface properties and structures on the hydrodynamics of a free pool and the overall effect on CHF,[22] investigation of the influence of capillary guiding structures for liquid has largely been limited to consideration of viscous flow resistance through the porous guides. In particular, liquid entrainment and intrusion in the vapor channels has not been investigated extensively.

This paper presents a novel manifold consisting of copper mesh that is oriented vertically and acts as a hierarchical wicking structure to control the flow of liquid and vapor above a horizontally oriented heated porous surface in boiling. Through this positioning and the differing wicking length scales at the manifold and heated surface, the copper mesh provides a low-resistance path for liquid replenishment to the heated surface while ensuring robust vertical separation of the liquid and vapor flow paths. Further exploiting the mesh structure and orientation, the novel liquid guide has a thin cross section that occludes less of the boiling surface than structures explored in the past.[43] The construction of the manifold additionally highlights the use of low-cost materials plus straightforward and scalable fabrication methods. The paper is organized as follows. The manifold design and construction are presented and the approach for heat transfer performance testing for an integrated manifold/wick system is described. Results for heat transfer behavior of the manifold/wick system are explored, including CHF and heat transfer coefficient values. We then analyze the various mechanisms influencing manifold performance, including liquid interaction with the vapor flow paths, and compare the performance to other systems in literature.

2. Approach

We evaluate the effectiveness of the mesh manifold in managing liquid delivery to and vapor escape from a heated porous surface in pool fed boiling in water.

2.1. Porous mesh guides for liquid delivery

In this paper, we present a passive pool fed boiling enhancement approach that separates vapor escape and liquid feeding with a metallic mesh manifold using capillary action. Fig. 1a schematically shows the manifold structure and function. Boiling occurs within the porous surface underneath the manifold. The copper mesh defines the flow path for liquid based on capillarity and guides it from the pool to the boiling surface of a heated porous wick. Spaces between the liquid channels present pathways for vapor escape. The liquid channels are distributed over the heat dissipation surface to minimize the distance the liquid must travel in the heated porous wick. Excess flow from the outer pool is restricted by solid walls at the edges of the manifold. The combination of the capillary suction of the mesh and the escaping vapor limit flooding liquid from the pool covering the heat transfer surface, reducing resistance for vapor escape. (However, some liquid flooding is likely present, as discussed later.) Liquid is driven to the heat dissipation surface primarily by the capillary suction of the wick, but there is also a gravitational driving force due to the difference in height between the liquid pool surface and the wick. To communicate the capillary suction of the fine porous features of the heated surface to the coarser mesh, they must achieve close contact to facilitate bridging of the liquid (Fig. 1a inset). Given the relatively high thermal resistance for conduction into the mesh, no appreciable boiling is expected within the mesh itself.

Fig. 1b is a micrograph of a portion of a manifold assembled with an AlN substrate with pin–fin surface enhancements. Fig. 1c shows an exploded view of the manifold. Liquid enters the mesh via plenums at either end of the channels that are open to the pool and travels along the mesh to the heated surface.

Three basic principles guide the design of the manifold: 1.) Establishing a pitch for the liquid channels similar to the estimated critical wicking distance for the porous structures (Fig. 1a)[20]; 2.) Maximizing liquid flow from the pool, through the channels, and to the heat dissipation surface; and 3.) Minimizing resistance for vapor escaping from the wick. These three objectives lead to multiple tradeoffs in the detailed design of the manifold. For example, a thicker liquid channel leads to lower liquid flow resistance but covers more of the wick and reduces the area available for vapor escape. Larger feature size for the liquid channel reduces liquid flow resistance but decreases the maximum capillary pressure that the liquid channel can support, limiting its ability to contain the liquid. These design choices also depend on the porous heat-dissipating surface. A thinner heated wick has higher potential critical heat flux due to a lower vapor resistance but also has a smaller critical wicking length, requiring reduced liquid channel spacing.[20] The result of balancing these design tradeoffs is a reduction in the competition between liquid and vapor flow, resulting in the dissipation of larger heat fluxes over large areas.

2.2. Manifold

The manifold is constructed from stacked layers of #100 copper mesh (250 μm thickness) and solid copper spacers. The spacers are chosen to provide 375-μm-wide vapor channels and 625–μm pitch between liquid channels. These spacings are chosen to minimize the

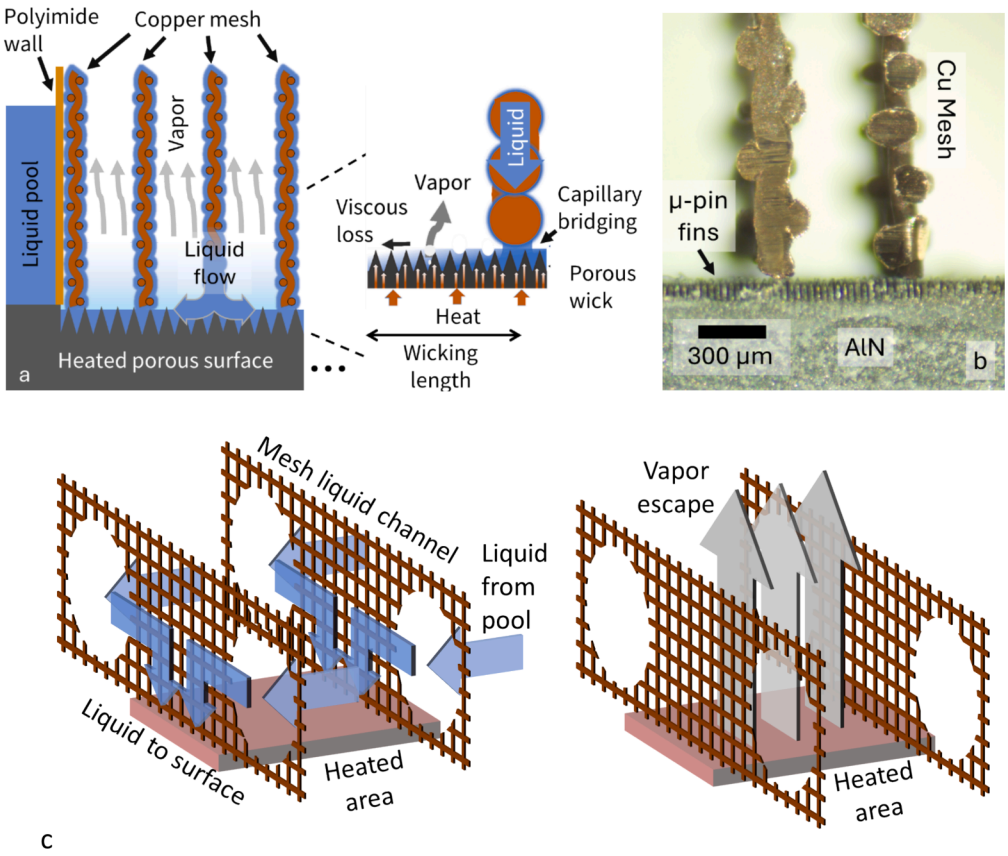

Fig. 1. Manifold structure and function. a.) Manifold cross section. Liquid is guided through mesh channels to the porous heat dissipation surface by capillary action where boiling occurs. Vapor escapes through the spaces between channels. The inset shows a magnified view of the manifold/wick interface. Liquid is drawn from the mesh by the high capillary pressure of the wick. Close contact between the manifold and wick is required to maintain a continuous liquid flow path. However, comparatively high thermal resistance between the wick and mesh minimizes boiling in the mesh. b.) Micrograph of assembled manifold/AlN substrate with porous surface enhancement. c.) Exploded oblique view of the manifold showing flow of liquid from the pool, through plenums, to the heated surface and vapor escape from the surface.

distance for liquid transport in the heated wick while maintaining a vapor channel width larger than the wire spacing of the mesh (254 μm), which is key to avoiding liquid saturation of vapor channels as discussed below. The layers are held together for convenience by compression applied via screws outside of the active area of the manifold, though monolithic manifolds have also been fabricated via sintering of the copper layers. The outer, impermeable layers of the manifold are formed from solid polyimide sheets. Fig. 2 shows a schematic of the manifold and component layers along with a photograph of an assembled manifold.

The final dimensions of the assembled manifold are 9 mm x 5.1 mm x 23 mm. The mesh structures are oriented perpendicular to the heat dissipation surface after manifold fabrication is complete, and the active footprint of the manifold on the heat dissipating wick is 5 mm x 5 mm. Fig. 2d shows the manifold placed normal to the wicking surface.

For liquid to enter the manifold, large cavities are created in the extremities of the manifold, forming plenums. Liquid enters the cavities through holes in the outer polyimide walls covered with copper mesh washers. The cavities also serve as through-holes for the assembly screws.

2.2.1. *Manifold materials*

The manifold uses plain weave copper mesh with a wire pitch of 100/inch (nominally 254 μm pitch). The wires have a diameter of ~ 114 μm, resulting in a minimum opening size of ~ 140 μm. The thickness of the mesh is approximately 250 μm. The capillary behavior of this mesh including maximum capillary pressure and permeability of the free-standing mesh has been measured previously.[47] The maximum capillary pressure in the mesh was found to be 1020 ± 20 Pa via an equilibrium capillary rise method, and the maximum permeability thickness product was measured to be 8×10^{-15} m^3. (The cross-sectional area for flow in the free-standing mesh is ambiguous, so the product of permeability and mesh thickness is the most appropriate characteristic of flow resistance for the mesh.).

Spacers defining the vapor channels are made of 127 μm thick copper. A polyimide sheet (127 μm thick) forms the wall between the manifold and the pool of water. Polyimide is chosen for its high temperature resistance and ease of processing. #2–56 stainless steel screws and nuts are used to hold the manifold together. Permeable washers, made of the same #100 copper mesh, are applied between the screws and the polyimide wall to allow liquid access to the plenums.

2.2.2. *Manifold fabrication*

The layers of the manifold are patterned using ultraviolet (UV) laser ablation. The performance of the manifold depends strongly on the capillary action of the mesh. Therefore, a clean and consistent surface is important. Before the manifold is assembled, the copper is chemically cleaned and etched to remove contaminants and provide a uniform surface. Organic residue on the mesh is removed via soaking in isopropyl alcohol, acetone, and then hexane in series. We then etch the mesh using 1% sulfuric acid for 40 min at 80 °C. After etching, the mesh is rinsed with water and cleaned again with isopropyl alcohol, acetone and then hexane. Once dry, the manifold layers are carefully stacked by hand. The stack consists of the following layers in order:

1.) Mesh washers, 2.) Polyimide wall, 3.) Copper mesh, 4.) Seven units of three copper shim spacers and one copper mesh (depicted in

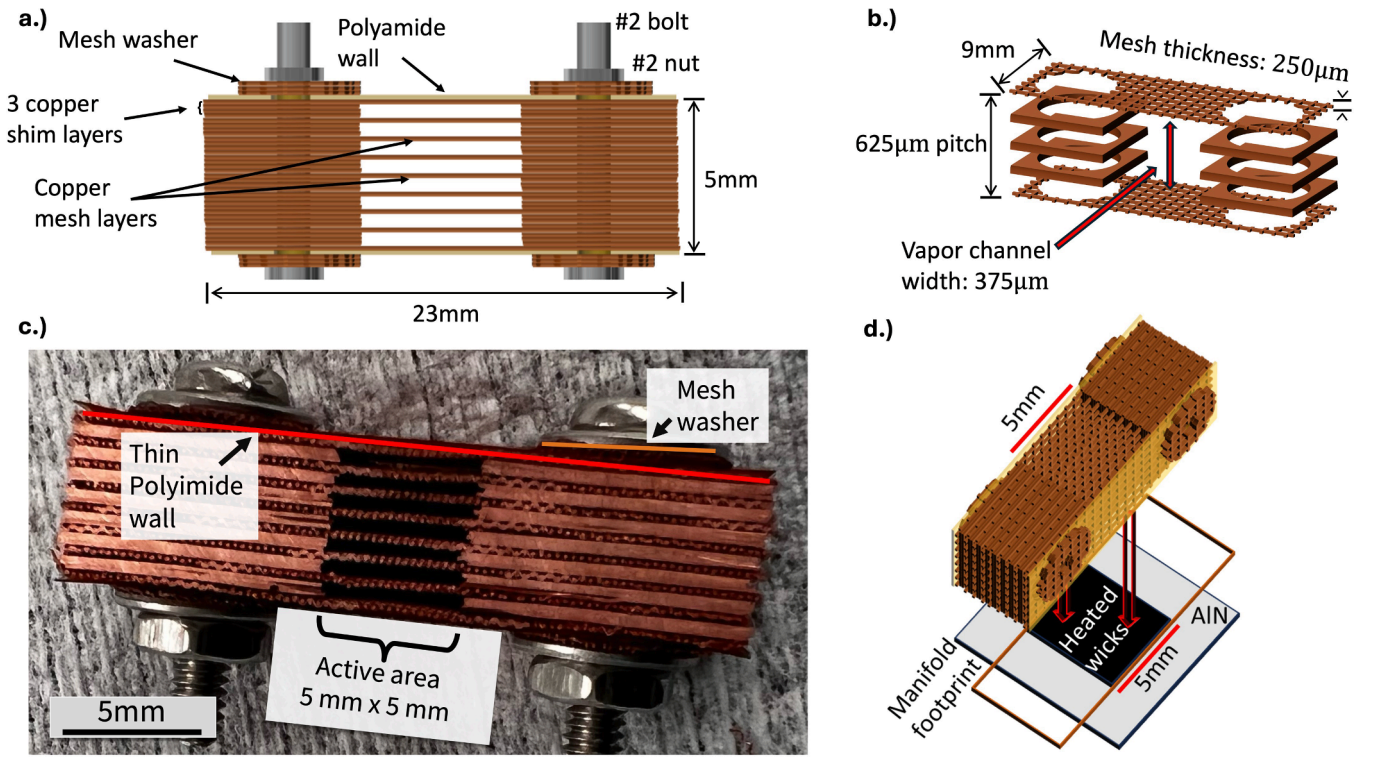

Fig. 2. Manifold construction a.) Top view schematic of assembled manifold. b.) Mesh and spacer configuration. c.) Assembled manifold as viewed from bottom (wick contact surface). Note planar polished bottom surface assuring uniform contact with the heated wick. d.) Schematic of copper mesh manifold showing the orientation above the heated wicking surface.

Fig. 2a), 5.) Polyimide sheet, 6.) Mesh washers.

Close contact between the manifold and wick is essential to operation, but the surface resulting from laser ablation is not highly planar. We planarize the bottom manifold surface (facing the heated wick) by grinding. To polish the manifold without deformation, the assembled manifold is embedded in Crystalbond 509 mounting adhesive. The embedded manifold is hand polished using a succession of finer grit SiC abrasive papers. Crystalbond is dissolved in acetone following grinding. After removal, the manifold is soaked in acetone overnight and then ultrasonically cleaned with fresh acetone to remove any remaining Crystalbond. Fig. 2c shows an assembled manifold. Manifolds are stored under vacuum desiccation between experiments to minimize accumulation of organic contaminants.

2.3. Enhanced boiling surface

The performance of the manifold is evaluated in conjunction with an enhanced boiling surface. Boiling occurs on the surface below the manifold while the copper mesh helps guide liquid and vapor paths. The capillary pressure from the wicking surface drives liquid flow through the copper mesh to replenish boiling.

2.3.1. Pin-fin surface

The manifold is mounted on a fine-featured boiling surface formed by UV laser ablation of an AlN substrate (shown in Fig. 3). The surface wicks are produced by a cross-hatching pattern using mild laser settings. [48] The resulting surface consists of a square array of conical pin fins. The pin fins have a pitch of 30 µm and height of approximately 110 µm. The wicks have a rough surface resulting from the laser ablation. Profilometry measurements indicate a surface roughness of 1.8 ± 0.5 µm on average. The high surface area and surface roughness of the AlN pin–fin microstructures enhance capillarity. The pores in between pillars serve as nucleation sites for boiling. The porous structure covers an area on the substrate of 5 mm x 5 mm. The AlN substrate (MTI Corp.) is initially

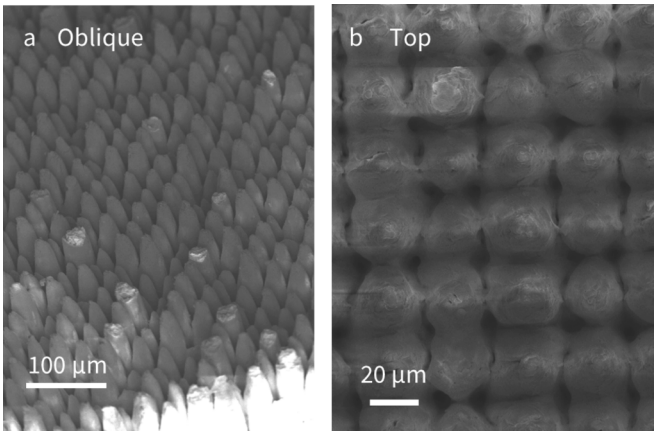

Fig. 3. Scanning electron microscopy images of porous microstructures on the heat dissipation surface crafted from aluminum nitride using a nano-second pulsed ultra-violet laser. The pin–fin micro-structures are conical in shape with approximate diameter of 30 µm and height of 110 µm.

0.635-mm-thick with a specified purity of 99 % and thermal conductivity specified as exceeding 170 W/m·K. The ablated surface is covered after laser processing to protect the features during mounting. No additional treatment is applied to the ablated surface prior to testing, and the wicks are maintained under vacuum desiccation between experiments. Transport in the wick is characterized via capillary rate of rise measurements [41,49] as detailed in supplementary information.

2.4. Thin film heater and temperature measurement

The porous surface is heated by a thin film resistor consisting of a titanium-platinum bilayer (25 nm titanium adhesion layer and 120 nm

platinum layer) with an area of 5 mm x 5 mm directly opposite the textured surface. To ensure that the thin film is stable during boiling experiments, the substrate is annealed for approximately 7 days at 155 °C. The platinum heater also serves as a resistance thermometer. Temperature is determined by resistance measurements across the heater and is calculated using the temperature coefficient of resistance (TCR) (see supplementary information section 1.2). Power dissipation from the heater is determined by the product of measured voltage and electrical current through the thin film. Fabrication of the heated surface has been discussed in detail in supplementary information section 1.

2.4.1. Heat loss and surface temperature corrections

The AlN substrate is insulated from below with silicone to minimize heat loss through modes other than boiling from the porous surface. Parasitic heat loss as a function of heater temperature is determined by measurement of steady-state dissipated power from a configuration with the manifold replaced by silicone insulation, preventing heat transfer from the wick surface. Heat flux reported here is corrected for parasitic heat losses by subtraction of the calculated heat loss at the measured heater temperature for each observation.

The temperature measured at the heater differs from the temperature presented at the wicking surface due to the thermal resistance of the aluminum nitride substrate. Temperatures reported for the boiling surface are calculated based on the measured heater temperature and heat flux, adjusting for conduction across the substrate. The temperature drop due to conduction is calculated assuming 1D conduction and the minimum specified substrate thermal conductivity (170 W/(m·K)) for the corrected heat flux (with parasitic loss excluded). Details of the parasitic heat loss characterization and heater temperature calculation are described in supplementary information section S1.2.

2.5. Testing procedure

The manifold is tested above a wicking surface acting in boiling in a nearly saturated pool of water open to the laboratory atmosphere. The wicking surface itself is also tested in pool boiling independently of the manifold.

2.5.1. Manifold mounting

The mounting of the manifold to the wick must be rigid and robust to maintain contact during boiling. Because an adhesive may clog the various porous structures in the system, we use a mechanical frame to hold the manifold in place. Fig. 4 shows a schematic of the boiling experimental setup. Additional figures detailing the setup, including standalone wick testing, are provided in supplementary information section 1.4.

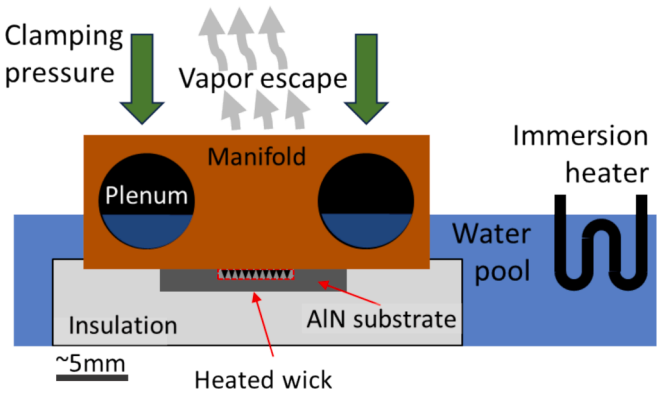

Fig. 4. Schematic of experimental assembly for pool boiling experiments with manifold over heated porous surface. Experiments are conducted in a pool of water heated near saturation by an immersion heater. Manifold contact to the heated AlN substrate is maintained by clamping by a polycarbonate frame. Temperature is measured at the bottom of the heater, opposite to the AlN wicks.

2.5.2. Pool boiling procedure

Testing is performed in a pool of water maintained near saturation temperature by immersion heaters. To minimize wave action near the manifold, immersion heaters are positioned well away from the manifold and a wire mesh barrier is used to suppress waves generated by boiling from the immersion heaters. Pool temperature is logged with a traceable Pt resistance temperature detector for use in calibration of heater temperature. During experiments, the pool temperature varies between 91–92.5 °C, due to fluctuations in the room ambient. The experiment is vented to the laboratory atmosphere. The pool temperature is limited to values somewhat below saturation by heat loss to the surroundings and the need for some separation distance between the immersion heaters and sample. During experiments, the level of the pool surface is maintained ~ 5 mm above the heated surface. Electrical current is supplied to the heater at incrementally increasing levels until critical heat flux is reached. CHF is defined by a rapid excursion in temperature. Once CHF is reached, the heater power is immediately removed. Current and voltage are logged at 100 Hz using a data acquisition system (Labjack T7pro). The heater resistance and power are found using Ohm's law. Heat flux is defined as the dissipated power divided by area. Additional details of the experimental procedure and data analysis are provided in supplementary information.

3. Results and discussion

The manifold separates the flow paths of liquid and vapor during the boiling process. This allows a significant increase in heat flux dissipation in pool fed boiling beyond that from the porous surface without further augmentation.

3.1. Heat transfer behavior

Fig. 5 shows the heat transfer performance for the manifold/wick system over five trials compared to the standalone porous surface for pool boiling in ambient atmosphere. The maximum CHF measured for the system with manifold is 490 W/cm^2 (with a range of 430 W/cm^2 to 490 W/cm^2 and an average of 462 W/cm^2). This represents a > 65 % increase compared to the bare wick, which dissipates 292 W/cm^2 for the best performing sample. The experimental trials in Fig. 5 are labeled in the order conducted. There is a notable increase in CHF and superheat from the first to final run, with each successive run resulting in an increased value. We interpret this change to be the result of corrosion of the copper and AlN surfaces by water resulting in more hydrophilic surfaces. It has been demonstrated that hydrophilicity improves wickability, a driving factor in CHF performance.[13] Corrosion of AlN in water is well established [50] and is also noted in experiments of the heated surface alone (see supplementary information). The AlN hydrolyses in contact with water, producing porous hydroxides of aluminum. The corrosion of AlN is greatly accelerated by boiling from the heated surface, so we expect the primary contribution to the corrosion of the AlN wick to come from the experimental time under heating, not simply exposure to the water pool.

3.1.1. Superheat

The maximum superheat measured at the boiling surface was ~ 36 °C. The measured temperature is an average of the entire heated area. Representative uncertainty in temperature is indicated in Fig. 5 and described in supplementary information section 2. We note that the primary contributions to this uncertainty are the pool temperature and heater TCR. Both these contributions affect the absolute but not the relative temperatures calculated. I.e., the data may be shifted along the x-axis, but the shape and relative position of the curves with respect to one another are not likely to be significantly changed. The remaining

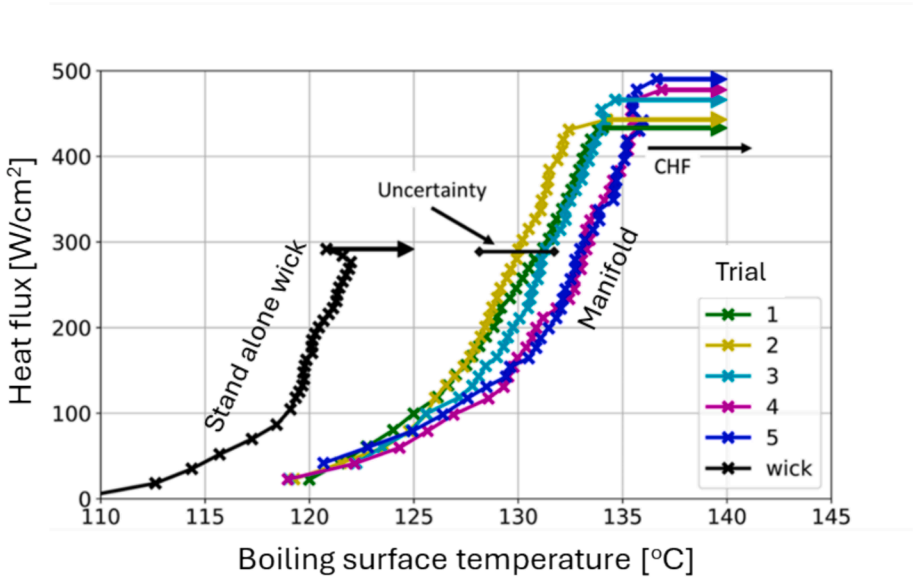

Fig. 5. Heat transfer performance for manifold/wick system for pool fed boiling in water at ambient pressure. Dissipated heat flux (corrected for parasitic loss) is presented versus boiling surface temperature (corrected for conduction through the substrate). Performance for a stand-alone heat dissipating wick is also shown. Five experimental runs on the same sample are presented and labeled in the order conducted.

uncertainty in temperature and the uncertainty in heat flux are both smaller than the symbol size. No estimate of uncertainty is included for the thermal conductivity of the substrate.

Fig. 6 depicts the heat transfer coefficient versus heat flux for the manifold/wick system. The heat transfer coefficient is measured as the heat flux corrected for parasitic heat losses divided by the superheat (relative to the 100 °C saturation temperature at ambient) at the wicking surface. The maximum heat transfer coefficient reached is 13.4 W/(cm^2·K) with a maximum differential heat transfer coefficient dq''/dT of 42 W/(cm^2·K). The standalone wick in comparison achieves a maximum heat transfer coefficient of 14.1 W/(cm^2·K). The absolute heat transfer coefficient is lower than the wick alone due to the higher superheat, as addressed below, but differential heat transfer coefficients are similar.

The superheat for the manifold/wick system is significantly increased compared to the wick alone. For similar heat fluxes, the superheat for the manifold system is ~ 10 °C higher. We believe the high superheat to be due to uneven flooding of the porous surface by the pool. We base this conclusion on experiments applying external suction via thin tubes introduced into the vapor channels as shown in Fig. 7 (and supplementary information section 1.5). Suction results in a mean decrease in superheat of > 2.5 °C over a wide range of heat fluxes, even for the relatively small area directly affected by the suction (emanating from 7 tubes with outer diameter of ~ 410 μm spread over the 5 mm x 5 mm boiling surface). Based on this result, we understand excess liquid flow from the pool to partially fill some vapor channels resulting in locally poor boiling performance. The liquid present above the boiling surface is held in place by the manifold creating resistance to vapor escape and insulating portions of the boiling surface (Fig. 7). Flooding may occur from gaps where the polyimide sidewalls meet the substrate, through the plenums, under the manifold, or from the edges of the manifold through the mesh. Suction also lowers the maximum observed CHF by ~ 12%, likely due to removal of liquid and obstruction of vapor escape paths.

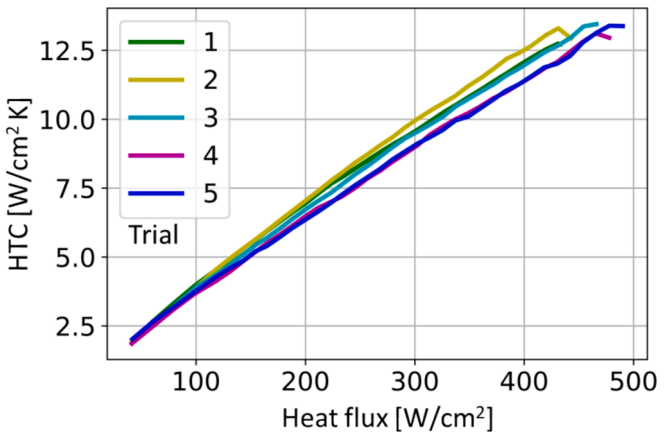

Fig. 6. Heat transfer coefficient for the manifold/wick system as a function of heat flux for pool fed boiling in water. Heat transfer coefficient is defined with respect to superheat above saturation. Five trials for the same sample are shown, labeled in the order performed.

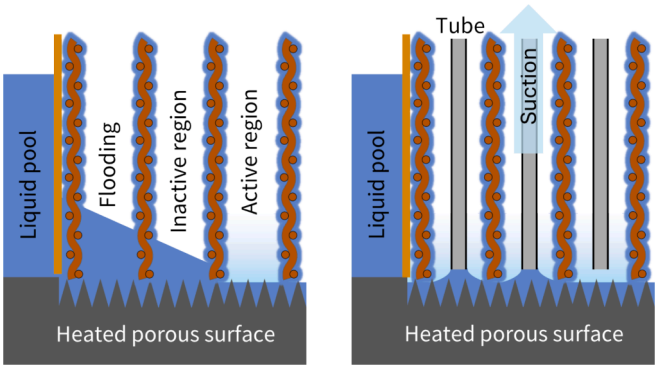

Fig. 7. Schematic of partial flooding of porous surface and action of suction. Local flooding is likely to drastically reduce the heat transfer from regions of the porous surface, resulting in elevated average temperature. Suction eliminates flooding locally, resulting in a reduction in surface temperature.

3.2. *Factors limiting maximum heat flux*

A variety of factors may limit the performance of the system in terms of maximum heat flux. We consider each of them here.

3.2.1. Heated wick performance

The heated wick itself may pose a limit. As discussed above, for thick wicks, resistance to vapor permeation through the wick may limit ultimate heat flux, but this is unlikely for the thin and open wick considered here. More relevant to the current case, there is a maximum heat flux that can be dissipated by the wick corresponding to the required lateral distance liquid must travel from the nearest reservoir (liquid channel) to the center of the evaporating region (vapor channel). Data correlating heat flux to maximum wicking distance is not available for the current pin–fin wick. However, thinner wicks with smaller feature sizes have been shown to support higher heat flux than observed here for wicking distances on the order of half the vapor channel width (~190 μm).[20]

3.2.2. Viscous flow resistance for liquid in the manifold mesh

Viscous drag for liquid in the mesh forming the manifold may also limit the maximum heat dissipation of the system. The liquid flow rate through the copper mesh is limited to that supported by the maximum capillary pressure sustained by the mesh. We expect an increase in the lateral transport distance in the mesh to result in lower CHF due to the increased viscous drag for liquid transiting the additional length. We have conducted experiments with manifolds having active areas of 10 mm x 5 mm over heated areas of 5 mm x 5 mm (i.e., with lateral transport distance doubled). These experiments show a CHF approximately 50% lower than the original (5 mm x 5 mm) design, potentially indicating effects of liquid viscous resistance in the mesh. However, we note that that other effects may influence this result.

Calculations of the flow driven by the maximum capillary pressure of the mesh (~1000 Pa) suggest higher potential heat flux. The one dimensional flow supported by meshes of various lengths and pressure gradients has been determined previously by integration of the mesh flow resistance and as a function capillary pressure along the flow direction.[47] For example, the mesh is calculated to support a superficial velocity of 6.8 mm/s (corresponding to a heat flux of 600 W/cm^2) over a mean distance of 10 mm,[47] which is significantly longer than the flow paths experienced in the current system.

One possible cause of the discrepancy between the observed and calculated mesh liquid flow capacity is the effect of vapor channel flooding, as discussed above. The increased perimeter of the larger-active-area manifold provides additional opportunities for uncontrolled liquid flow from the pool, leading to additional flooding, which may clog the vapor channels preventing vapor escape, as considered below. Additionally, non-ideal contact between the mesh channel and the wick below may influence liquid flow performance. Gaps between these two elements may allow vapor intrusion and prevent liquid bridging, raising the fluid flow resistance into the wick, as mentioned below. We do note significant variability in performance for manifolds poorly seated on the wick.

3.2.3. Viscous flow resistance for vapor in the manifold

Vapor escape is essential to the functioning of the system. For the maximum heat flux measured, the Reynolds number for the escaping vapor is ~ 110, and the resistance to vapor escape can be approximated based on laminar flow between parallel plates,[51]

$$\Delta p = u_{vap} h \frac{12\mu_{vap}}{\delta_{vap}^2} \tag{1}$$

where h is the height of the manifold, δ_{vap} is the width of the vapor channel, and μ_{vap} is the dynamic viscosity of the vapor. For the manifold operating at a heat flux of 450 W/cm^2, the vapor experiences a pressure drop of ~ 50 Pa.

This small pressure has minimal effect on the phase-change process. From the Clausius–Clapeyron slope, this corresponds to a saturation temperature change of ~ 0.01 °C. The pressure of the vapor can impact the flow of liquid in the mesh, via the capillary pressure. The capillary pressure is the difference between the external vapor pressure and the internal liquid pressure. As the vapor pressure at the bottom of the channel increases to supply larger vapor flow, the capillary pressure at the bottom of the mesh correspondingly increases. However, the calculated change in vapor pressure across the height of the manifold is unlikely to significantly affect the resistance of the mesh to liquid flow. Previous characterization shows that significant change in permeability does not occur until capillary pressures of above 600 Pa.[47] The contact surface between the manifold and meshes may be particularly sensitive to intrusion of vapor. Therefore, the manifold and wick must mate without significant gaps to maintain a capillary bridge between the two. In the current implementation, this is achieved by polishing the lower manifold surface to ensure planarity.

Despite the low pressure drop in the vapor channel, the interaction between vapor and liquid flows may still have a meaningful impact on manifold performance. Although the porous guides reduce the competition between liquid and vapor flow, there is still an interaction at the liquid channel surface, where the fast-moving vapor exerts a drag on the liquid. The shear from the vapor can drive the liquid away from the heat dissipation surface. At sufficiently high vapor velocities, this action may result in entrainment of liquid droplets in the vapor flow. We have imaged the ejection of liquid droplets from the manifold, Fig. 8. However, we are not able to quantify the effect on liquid flow. Entrainment is a known limitation in the operation of thermosyphons and heat pipes, including those with mesh wicks; however, the significance for capillary-driven heat pipes has been questioned.[21]

The relative magnitude of the shear stress compared to the capillary action of the mesh can be quantified by the Weber number. For the mesh wire pitch (~250 μm) and vapor velocity corresponding to 450 W/cm^2 heat flux, the Weber number is ~ 0.075. Models developed for heat pipes suggest a critical Weber number of ~ 1 for entrainment to become significant.[21] It is possible that significant surface flow on the mesh is more sensitive to shear from the vapor than the mesh/solid wall configuration usually treated in heat pipes.

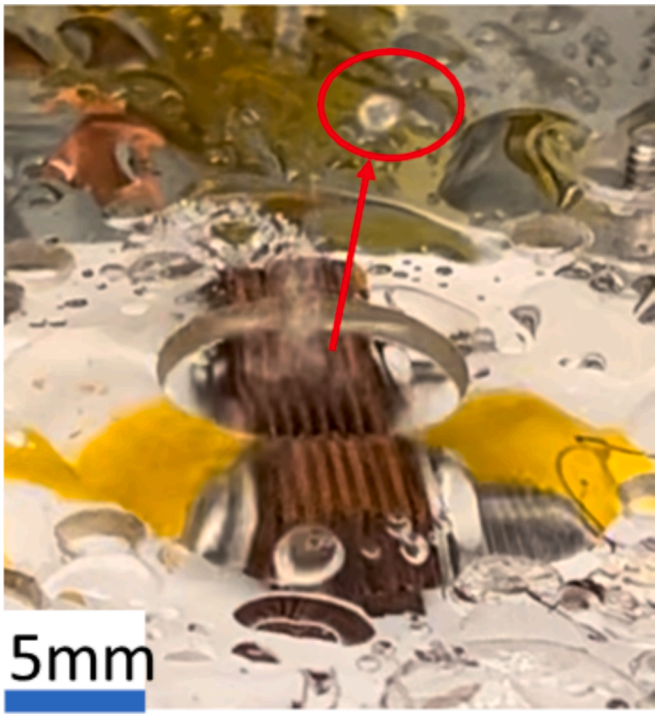

Fig. 8. Liquid ejection from manifold due to vapor flow at higher heat flux. A liquid droplet (circled in red) is shown along with additional liquid ejection (blurred area to left of arrow). (For interpretation of the references to colour in this figure legend, the reader is referred to the web version of this article.)

3.2.4. Liquid intrusion in the vapor channel

In addition to the vapor flow resistance provided by the mesh channels, liquid may be present in the vapor channels beyond the flooding of the heated surface discussed above. This state results in a complex two-phase condition in the vapor channels, with a very high resistance to vapor flow expected. The vapor channels are completely flooded at startup and only cleared once there is sufficient vapor flow to force the liquid out. Due to the larger vapor channel width (~400 μm) compared to the feature size of the mesh itself (~250 μm), we anticipate that the vapor channels are mostly clear at capillary pressures where the mesh retains liquid. However, we cannot directly determine the distribution of liquid in the vapor channel. The presence of liquid in the vapor channels may account for the ejection of droplets from the manifold, despite the small Weber number. Importantly, liquid bridging in the vapor channel is the primary limit on the minimum width of the vapor channel. Reduced liquid channel spacing would reduce the required liquid flow per channel and enhance CHF. However, at vapor channel widths similar to or smaller than the mesh feature size, the vapor channel would be expected to robustly retain liquid, eliminating the phase separation function of the manifold. We note that the hydrostatic pressure of the water at the pool height of ~ 5 mm above the heated surface is similar to the viscous pressure predicted for vapor escape (~50 Pa).

3.3. Temperature stability

We have focused on the steady-state behavior of the manifold/wick system, but the manifold also influences the transient behavior. The manifold provides a steady supply of liquid to the heat dissipation surface. In comparison, surfaces undergoing normal pool boiling experience significant local excursions in temperature as bubbles form, grow, and depart. This effect is especially dramatic as the surface approaches CHF.

Due to the small thermal mass of the system, we can directly observe thermal transients. Fig. 9 shows a histogram of instantaneous temperature observations over ~ 40 s at each heat flux. As heat flux increases, the stability improves somewhat until heat fluxes near CHF are reached. This is in contrast to unaided pool boiling which shows significant instability as the transition boiling regime is approached.

3.4. Comparison to other works

Table 1 provides examples of related studies applying approaches to guide liquid and vapor flow in pool boiling using water along with representative performance metrics.

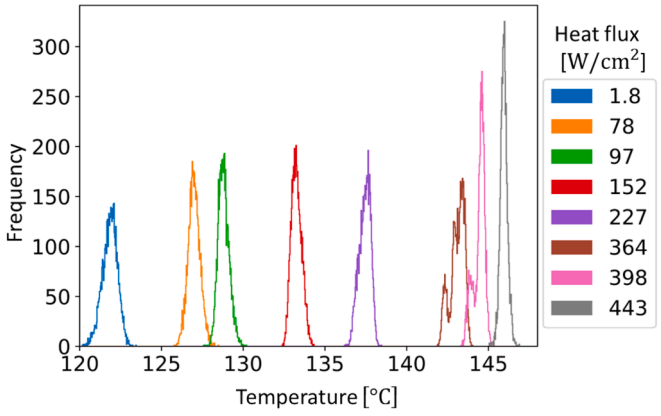

Fig. 9. Temperature variation of heated surface in manifold/wick system at various dissipated heat fluxes for pool boiling in water. Frequency of instantaneous temperature observations over 40 s periods are reported for each heat flux.

Table 1
Comparison of structures to direct liquid and vapor flow in pool boiling with water.

Reference	Approach	Area	Performance
This study	Mesh manifold above pin fin array	5 mm x 5 mm	CHF: 490 W/cm^2 HTC: 13.4 W/(cm^2·K)
Mori et al. [46]	Honeycomb porous plate over surface with nanoparticle depositions	7 cm^2	CHF: 320 W/cm^2 HTC: 14.5 W/(cm^2·K)
Pastuszko et al[39]	Surface-wicks in combination with perforated metal foil and wire mesh	26.5 mm x 26.5 mm	CHF: 46 W/cm^2 HTC: 3.5 W/(cm^2·K)
Long et al [40]	Laser patterned hierarchical wicking structures	20x20 mm^2	CHF: 239.4 W/cm^2 HTC: 26.0 W/(cm^2·K)
Sun et al. [42]	Sintered copper mesh/particle hierarchical wicking structures	5.75 cm^2	CHF: 242.4 W/cm^2 HTC: 19.0 W/(cm^2·K)
Zhong et al. [52]	Copper nano-particle and mesh bi-layer	7.1 cm^2	CHF: 80 W/cm^2 HTC: 9.81 W/(cm^2·K)
Rahman et al.[53]	Low conductivity strips in copper surface	1 cm^2	CHF: 230 W/cm^2 HTC: 21.0 W/(cm^2·K)
Xie et al. [27]	Various bi-conductive configurations	20x20 mm^2	CHF: 114 W/cm^2 HTC: 6.7 W/(cm^2·K)
Haji et al. [29]	Bi-philic surfaces using SiO_2 particles	3.46 cm^2	CHF: 108.8 W/cm^2 HTC: 12.6 W/(cm^2·K)
Shim, et al. [30]	Super bi-philic surface using silicon nanowires and fluoro-octyltrichloro silane superhydrophobic dots	10x10 mm^2	CHF: 166 W/cm^2 HTC: 33 W/(cm^2·K)

Mori et al. studied a nanoparticle coated surface in combination with a porous plate.[46] The use of porous guides to control liquid–vapor flow configuration was similar to the current work, but the guides had a much smaller pore size with a median pore radius of 130 nm. Consequently, the guides provided much stronger capillary suction to contain liquid but required larger thicknesses (0.45 mm) to convey liquid due to the higher flow resistance of the fine pore structure. The pool boiling configuration included a pool height above the top of the guides.

A number of studies have specifically applied mesh or similar constructions in combination with porous structures to form hierarchical systems to control liquid and vapor flow in boiling. Pastuszko et al. added mesh or perforated plates above pin fin arrays with boiling tests performed in water, ethanol, FC-72, and Novec 649.[39] Sun et al. created hierarchical sintered copper pillars on mesh with the surface further treated to form nanoscale porosity.[42] Zhong et al. created a hierarchal boiling surface with very low incipience to boiling and high heat transfer effectiveness at low heat flux.[52] Mesh is welded on top of nanoparticles in this implementation. These studies use meshes that are oriented parallel to the heated surface limiting the effect on the liquid and vapor flow to near the heated surface compared to the orthogonally oriented mesh in the current manifold.

Rahman, et al. increased the heat transfer performance in pool boiling by adding low conductivity material to the surface (bi-conductive).[53] In research on bi-conductive boiling surfaces, Xie et al. studied the influence of the pattern on performance.[27] Mixed wettability surfaces (bi-philic) were studied in Haji et al. to increase boiling

effectiveness.[29] Super bi-philic surfaces were studied by Shim, et al. [30] to further increase boiling performance. A hierarchical structure modeled after a rose petal is studied by Long et al. to reach high wettability and heat transfer effectiveness.[40] Similar to this work, the wicking surface is made with laser ablation.

The current approach shows the highest CHF of the methods considered in Table 1. However, we note an important difference between the pool boiling configurations of the other work and the current approach. The current manifold relies on lateral feeding of the liquid. This lateral transport potentially places limits on the dimensions of the cooled area along the liquid channels. Such limitations are not present for liquid fed from the pool directly above the heated surface. The lateral transport of liquid in the current work is in some ways akin to edge fed capillary driven boiling systems. As such, we also compare the current approach with capillary fed systems in Table 2 below.

Hwang, et al. [54] constructed a converging multi-artery wick for improved lateral liquid supply while allowing heat to dissipate over a larger area. Sudhakar et al.[38] created a two-layer wick with separate paths for liquid supply and vapor escape. Semenic & Catton [37] examined bi-porous wicks formed from particle clusters. Ju, et al. [34] explored monolayers of Cu particles combined with columnar arteries, converging lateral arteries, and bi-porous structures. Ryu et al. [36] applied a metal foam liquid supply layer over nanostructure enhanced micro-pin fin array. Cai & Bhunia [32] created a bi-porous wick formed from patterned carbon nano tube forests. Lv & Li [35] tested a multilayer super-hydrophilic mesh wick in heat pipe. The current work is comparable in CHF performance to many of the edge fed wicks, but generally shows less variability in temperature at high heat fluxes where the edge fed wicks commonly experience partial dryout.

4. Conclusion

The application of a mesh manifold can dramatically increase the critical heat flux of a porous surface operating in pool boiling. The manifold allows even distribution of liquid to the heat dissipation surface to minimize liquid transport distances within the heated porous structure. This effect also reduces the competition between liquid delivery to and vapor escape from the heated surface. The copper mesh manifold described here, when combined with an AlN micro-pin fin wick, shows a critical heat flux up to 490 W/cm^2, a $>$ 65 % increase in CHF performance over the pin–fin array alone. The maximum heat transfer coefficient of 13.4 W/(cm^2·K) for the combined system is somewhat lower than the maximum value for the porous surface alone a (14.1 W/(cm^2·K)). This reduced performance is attributed to liquid intrusion into the defined vapor channels of the manifold.

Table 2
Comparison of structures fed from the perimeter in capillary fed boiling.

Reference	Approach	Area	Performance
This study	Mesh manifold above pin fin array	5 mm x 5 mm	CHF: 490 W/cm^2 HTC: 13.4 W/(cm^2·K)
Hwang, et al. [54]	Porous artery structure of varying thickness	1 cm x 1 cm	CHF: 580 W/cm^2
Sudhakar et al. [38]	Two layer wick with separate liquid supply path.	1 cm x 1 cm	CHF: 485 W/cm^2
Semenic& Catton [37]	Bi-porous wicks	0.7 cm^2	CHF: 990 W/cm^2
Ju, et al. [34]	Hybrid wick configurations with various liquid supply structures.	4 cm^2	CHF: 550 W/cm^2 HTC: 13.3 W/(cm^2·K)
Ryu et al. [36]	Hierarchical wick	4 mm x 4 mm	CHF: 400 W/cm^2 HTC: $>$ 6 W/(cm^2·K)
Cai & Bhunia [32]	patterned carbon nano tube forests.	2 mm x 2 mm &10 mm x 10 mm	CHF: 770 W/cm^2& CHF: 160 W/cm^{2}respectively
Lv & Li [35]	Multilayer superhydrophilic mesh wick.	Two 5 mm x 2 mm heaters	CHF: 490 W/cm^2 HTC: 25.64 W/(cm^2·K)

The manifold builds on existing works applying a variety of methods to define the flow of liquid and vapor above a surface acting in pool boiling (e.g. see [15] and introduction). These methods have also included porous guides for liquid flow toward the surface.[43] Resistance of the porous structures was identified as an important characteristic of liquid guides. There is thus a need to search for low resistance guides that do not occlude excessive portions of the boiling surface. The mesh considered here provides a relatively low flow resistance as previously characterized.[47] However, reducing guide resistance in general implies lower capillary pressure serving to isolate the liquid and vapor flows. These and other effects limiting performance have been identified along with tradeoffs in terms of guide characteristics and placement. Despite the presence of the liquid pool and some gravitation drive of the liquid flow in the currently presented configuration, we note the similarity of action of the manifold/wick system to that of a heat pipe, as long as the guides are effective in containing the liquid and the pool is sufficiently shallow so as not to cover the vapor escape paths.

Importantly, the action of the manifold is largely independent of the heated porous surface. Therefore, a range of porous surfaces are applicable. The key design consideration is maintaining mesh spacings as close to the critical wicking length of the surface as practicable.[20] This may in turn influence mesh spacing to maintain higher capillary pressure in the mesh than the adjacent vapor channel for separation of flows.

The relative independence of manifold and surface has important implications for durability. Aluminum nitride, as used here, is known to corrode in water. Methods have been described to enhance its durability in phase change heat transfer applications.[55] However, as the manifold is independent of the wick, different, more durable and established materials such as copper are also applicable for the underlying wick. Furthermore, the mechanisms of action of the manifold apply to other fluids, such as dielectric fluids commonly used in immersion cooling of electronics.[56,57] Given the similarity of the mechanisms with heat pipes, we can expect a similar dependence of performance on the thermophysical working fluid properties as expressed in the fluid's figure of merit.

The manifold construction involves simple, readily available materials and fabrication techniques. Pool fed boiling is a commonly applied phase-change cooling approach, and the mesh manifold allows enhancement without significant redesign of existing systems. The lack of a pump and maintenance, compared to traditional microfluidic manifolds, reduces system complexity, and improves reliability. A recent techo-economic analysis has shown the cost benefits of the mesh manifold approach compared to micromachining methods traditionally applied to microfluidic systems.[4] Potential applications for the copper mesh manifold include stationary high-heat-flux electronics (e.g. power generation and transport), as the pool needs to be level during operation to prevent flooding of the vapor escape paths from the top. We note that immersion cooling of electronics has been extensively applied.[56,57] The current manifold design could be added to the surface of existing packages with porous enhancement applied.

Design parameters for the current implementation of the manifold are largely chosen out of convenience and knowledge of similar systems. However, the key mechanisms influencing performance have been identified, and there remains significant opportunity for optimization. Promising directions for future work include: optimization of the liquid channel spacing using porous substrates with well-characterized critical wicking lengths; further investigation of the role of liquid intrusion in the vapor channel via variation of vapor channel width, mesh capillary suction, and perimeter sealing; and optimization of mesh geometry to balance permeability and liquid retention.

Declaration of competing interest

The authors declare the following financial interests/personal relationships which may be considered as potential competing interests: Roman Giglio, Muhammad R. Shattique, Sreekant Narumanchi, Mehdi Asheghi, Kenneth E. Goodson, and James W. Palko report financial support was provided by Advanced Research Projects Agency-Energy. Ercan M. Dede, Roman Giglio, Muhammad R. Shattique, Sreekant Narumanchi, Mehdi Asheghi, Kenneth E. Goodson, and James W. Palko have patent #US11729951B2 issued to Denso Corp, Toyota Motor Corp, Mirise Technologies Corp, University of California-Merced, Leland Stanford Junior University, Alliance for Sustainable Energy LLC. If there are other authors, they declare that they have no known competing financial interests or personal relationships that could have appeared to influence the work reported in this paper.

Acknowledgments

This research was supported by funding from the Advanced Research Projects Agency-Energy (ARPA-E), an agency of the United States Government, U.S. Department of Energy, under Award Number DE-AR0001055 in the OPEN program monitored by Dr. Peter de Bock. The authors acknowledge the Imaging and Microscopy Facility (IMF) at UC Merced (funded under NSF EAR Award number: 0420982). This paper's views, opinions, and findings are those of the authors. This work was co-authored by the National Renewable Energy Laboratory (NREL), operated by Alliance for Sustainable Energy, LLC, for the U.S. Department of Energy (DOE) under Contract No. DE-AC36-08GO28308. This work was supported by ARPA-E funding. The views expressed in the article do not necessarily represent the views of the DOE or the U.S. Government. The U.S. Government retains and the publisher, by accepting the article for publication, acknowledges that the U.S. Government retains a nonexclusive, paid-up, irrevocable, worldwide license to publish or reproduce the published form of this work, or allow others to do so, for U.S. Government purposes.

Appendix A. Supplementary material

Supplementary data to this article can be found online at https://doi.org/10.1016/j.applthermaleng.2024.124918.

Data availability

Data will be made available on request.

References

[1] S. M. Sohel Murshed and C. A. Nieto de Castro, "A critical review of traditional and emerging techniques and fluids for electronics cooling," *Renewable & sustainable energy reviews*, vol. 78, no. C, pp. 821–833, Oct. 2017, doi: 10.1016/j.rser.2017.04.112.

[2] A. Bar-Cohen, et al., The ICECool fundamentals effort on evaporative cooling of microelectronics, IEEE Trans. Compon. Packag. Manuf. Technol. (2021), https://doi.org/10.1109/TCPMT.2021.3111114.

[3] J.W. Palko, et al., Approaching the limits of two-phase boiling heat transfer: High heat flux and low superheat, Appl. Phys. Lett. 107 (25) (Dec. 2015), https://doi.org/10.1063/1.4938202.

[4] E. M. Dede *et al.*, "Techno-economic feasibility analysis of an extreme heat flux micro-cooler.," 2023, *Cell Press, [Cambridge, MA] :* doi: 10.1016/j.isci.2022.105812.

[5] A. Bar-Cohen[1], J. J. Maurer, and J. G. Felbinger, "DARPA's intra/interchip enhanced cooling (ICECool) program," in *CS MANTECH Conference, May 13th-16th*, 2013.

[6] Y. L. Chen and C. C. Lee, "Strength of solid-state silver bonding between copper," *Proceedings - Electronic Components and Technology Conference*, no. May 2013, pp. 1773–1776, 2013, doi: 10.1109/ECTC.2013.6575815.

[7] V.P. Carey. *Liquid Vapor Phase Change Phenomena: An Introduction to the Thermophysics of Vaporization and Condensation Processes in Heat Transfer Equipment*, Second Edition, Taylor & Francis, 2007.

[8] M.M. Rahman, M. McCarthy, Boiling enhancement on nanostructured surfaces with engineered variations in wettability and thermal conductivity, Heat Transf. Eng. 38 (14–15) (2017) 1285–1295, https://doi.org/10.1080/01457632.2016.1242961.

[9] G. Liang, I. Mudawar, Pool boiling critical heat flux (CHF) – Part 1: Review of mechanisms, models, and correlations, Int. J. Heat Mass Transf. 117 (Feb. 2018) 1352–1367, https://doi.org/10.1016/J.IJHEATMASSTRANSFER.2017.09.134.

[10] G. Liang, I. Mudawar, Pool boiling critical heat flux (CHF) – Part 2: Assessment of models and correlations, Int. J. Heat Mass Transf. 117 (Feb. 2018) 1368–1383, https://doi.org/10.1016/J.IJHEATMASSTRANSFER.2017.09.073.

[11] B. Novak Zuber and L. Angeles, "On the Stability of Boiling Heat Transfer," *J Fluids Eng*, vol. 80, no. 3, pp. 711–714, Apr. 1958, doi: 10.1115/1.4012484.

[12] S.G. Kandlikar, A theoretical model to predict pool boiling CHF incorporating effects of contact angle and orientation, J. Heat Transf. 123 (6) (Dec. 2001) 1071–1079, https://doi.org/10.1115/1.1409265.

[13] M.M. Rahman, E. Ölçeroglu, M. McCarthy, Role of wickability on the critical heat flux of structured superhydrophilic surfaces, Langmuir 30 (37) (2014) 11225–11234, https://doi.org/10.1021/la5030923.

[14] G. Liang, I. Mudawar, Review of pool boiling enhancement by surface modification, Int. J. Heat Mass Transf. 128 (Jan. 2019) 892–933, https://doi.org/10.1016/J.IJHEATMASSTRANSFER.2018.09.026.

[15] S. Mori, Y. Utaka, Critical heat flux enhancement by surface modification in a saturated pool boiling: A review, Int. J. Heat Mass Transf. 108 (May 2017) 2534–2557, https://doi.org/10.1016/J.IJHEATMASSTRANSFER.2017.01.090.

[16] H. Moghadasi, H. Fathalizadeh, A. Mehdikhani, H. Saffari, Surface modification utilizing photolithography process for pool boiling enhancement: An experimental study, Heat Transf. Eng. 43 (12) (Jul. 2022) 1008–1024, https://doi.org/10.1080/01457632.2021.1932037.

[17] A. Mehdikhani, H. Moghadasi, H. Saffari, An experimental investigation of pool boiling augmentation using four-step electrodeposited micro/nanostructured porous surface in distilled water, Int. J. Mech. Sci. 187 (2020) 105924, https://doi.org/10.1016/j.ijmecsci.2020.105924.

[18] A. Haji, H. Moghadasi, H. Saffari, Experimental study of electrospray deposition method parameters on TiO_2 coating structure in pool boiling performance enhancement, Exp. Heat Transf. 35 (7) (Nov. 2022) 1038–1058, https://doi.org/10.1080/08916152.2021.2019146.

[19] Z. Lv, Y. An, C. Huang, Enhanced pool boiling heat transfer by adding metalized diamond in copper porous materials, Appl. Therm. Eng. 226 (2023) 120288, https://doi.org/10.1016/j.applthermaleng.2023.120288.

[20] C. Zhang, J.W. Palko, M.T. Barako, M. Asheghi, K.E. Goodson, Design and optimization of well-ordered microporous copper structure for high heat flux cooling applications, Int. J. Heat Mass Transf. 173 (Jul. 2021) 121241, https://doi.org/10.1016/J.IJHEATMASSTRANSFER.2021.121241.

[21] A. Faghri. *Heat Pipe Science And Technology*, Taylor \& Francis, 1995.

[22] S.G. Liter, M. Kaviany, Pool-boiling CHF enhancement by modulated porous-layer coating: theory and experiment, Int. J. Heat Mass Transf. 44 (22) (Nov. 2001) 4287–4311, https://doi.org/10.1016/S0017-9310(01)00084-9.

[23] M.M. Rahman, J. Pollack, M. McCarthy, Increasing boiling heat transfer using low conductivity materials, Sci. Rep. 5 (1) (Aug. 2015) 13145, https://doi.org/10.1038/srep13145.

[24] J. Yin, X. Xiao, L. Feng, K. Zhong, H. Jia, Experimental investigation of pool boiling characteristics of surfactant solutions on bi-conductive surfaces, Int. J. Heat Mass Transf. 157 (Aug. 2020) 119914, https://doi.org/10.1016/J.IJHEATMASSTRANSFER.2020.119914.

[25] A. Heidary, H. Moghadasi, H. Saffari, Impact of dimensional characteristics of low-conductive channels on the enhancement of pool boiling: An experimental analysis, Int. J. Mech. Sci. 209 (2021) 106710, https://doi.org/10.1016/j.ijmecsci.2021.106710.

[26] A. Heidary, H. Moghadasi, H. Saffari, On the influences of low-conductive channels in the pool boiling amendment: Empirical investigation with providing correlation, Therm. Sci. Eng. Prog. 36 (2022) 101484, https://doi.org/10.1016/j.tsep.2022.101484.

[27] T. Xie, Y. Utaka, Z. Chen, T. Hirotani, S. Mori, Effect of material arrangement pattern on different-mode-interacting boiling in narrow gaps with two liquid supply systems, Appl. Therm. Eng. 191 (Jun. 2021) 116893, https://doi.org/10.1016/J.APPLTHERMALENG.2021.116893.

[28] A.R. Betz, J. Xu, H. Qiu, D. Attinger, Do surfaces with mixed hydrophilic and hydrophobic areas enhance pool boiling? Appl. Phys. Lett. 97 (14) (Oct. 2010) 141909 https://doi.org/10.1063/1.3485057.

[29] A. Haji, H. Moghadasi, H. Saffari, Enhanced boiling heat transfer efficiency through the simultaneous use of electrospray and photolithography methods: An experimental study and correlation, Therm. Sci. Eng. Prog. 38 (2023) 101661, https://doi.org/10.1016/j.tsep.2023.101661.

[30] D. Il Shim, W. T. Hsu, M. Yun, D. Lee, B. S. Kim, and H. H. Cho, "Superbiphilic patterned nanowires with wicking for enhanced pool boiling heat transfer," *Int J Mech Sci*, vol. 249, p. 108280, Jul. 2023, doi: 10.1016/J.IJMECSCI.2023.108280.

[31] W. Zhang, Y. Chai, J. Xu, G. Liu, Y. Sun, 3D heterogeneous wetting microchannel surfaces for boiling heat transfer enhancement, Appl. Surf. Sci. 457 (Nov. 2018) 891–901, https://doi.org/10.1016/J.APSUSC.2018.07.021.

[32] Q. Cai, A. Bhunia, High heat flux phase change on porous carbon nanotube structures, Int. J. Heat Mass Transf. 55 (21) (2012) 5544–5551, https://doi.org/10.1016/j.ijheatmasstransfer.2012.05.027.

[33] G.S. Hwang, et al., Multi-artery heat-pipe spreader: Lateral liquid supply, Int. J. Heat Mass Transf. 54 (11) (2011) 2334–2340, https://doi.org/10.1016/j.ijheatmasstransfer.2011.02.029.

[34] Y.S. Ju, et al., Planar vapor chamber with hybrid evaporator wicks for the thermal management of high-heat-flux and high-power optoelectronic devices, Int. J. Heat

Mass Transf. 60 (2013) 163–169, https://doi.org/10.1016/j.ijheatmasstransfer.2012.12.058.
[35] L. Lv, J. Li, Managing high heat flux up to 500W/cm2 through an ultra-thin flat heat pipe with superhydrophilic wick, Appl. Therm. Eng. 122 (2017) 593–600, https://doi.org/10.1016/j.applthermaleng.2017.05.050.
[36] S. Ryu, J. Han, J. Kim, C. Lee, Y. Nam, Enhanced heat transfer using metal foam liquid supply layers for micro heat spreaders, Int. J. Heat Mass Transf. 108 (2017) 2338–2345, https://doi.org/10.1016/j.ijheatmasstransfer.2017.01.071.
[37] T. Semenic, I. Catton, Experimental study of biporous wicks for high heat flux applications, Int. J. Heat Mass Transf. 52 (21) (2009) 5113–5121, https://doi.org/10.1016/j.ijheatmasstransfer.2009.05.005.
[38] S. Sudhakar, J.A. Weibel, F. Zhou, E.M. Dede, S.V. Garimella, Area-scalable high-heat-flux dissipation at low thermal resistance using a capillary-fed two-layer evaporator wick, Int. J. Heat Mass Transf. 135 (2019) 1346–1356, https://doi.org/10.1016/j.ijheatmasstransfer.2019.02.075.
[39] R. Pastuszko, R. Kaniowski, T.M. Wójcik, Comparison of pool boiling performance for plain micro-fins and micro-fins with a porous layer, Appl. Therm. Eng. 166 (2020) 114658, https://doi.org/10.1016/j.applthermaleng.2019.114658.
[40] J. Long, Z. Liu, Z. Cao, J. Wu, X. Xie, Highly efficient pool boiling heat transfer on surfaces with zoned rose-petal-inspired hierarchical structures, Appl. Therm. Eng. 241 (2024) 122330, https://doi.org/10.1016/j.applthermaleng.2023.122330.
[41] J. Wu, J. Lin, Y. Yan, Z. You, Z. Su, J. Long, Grooved-porous composite wick structures for highly efficient capillary-fed boiling heat transfer, Appl. Therm. Eng. 256 (2024) 124029, https://doi.org/10.1016/j.applthermaleng.2024.124029.
[42] Y. Sun, et al., Hierarchical sintered porous surfaces with enhanced pool boiling heat transfer performance for high-power cooling applications, Appl. Therm. Eng. 249 (2024) 123368, https://doi.org/10.1016/j.applthermaleng.2024.123368.
[43] S. Mori, K. Okuyama, Enhancement of the critical heat flux in saturated pool boiling using honeycomb porous media, Int. J. Multiphase Flow 35 (10) (Oct. 2009) 946–951, https://doi.org/10.1016/J.IJMULTIPHASEFLOW.2009.05.003.
[44] W. Fogaça, S. Mori, K. Imanishi, K. Okuyama, J.R.C. Piqueira, Effect of honeycomb porous plate on critical heat flux in saturated pool boiling of artificial seawater, Int. J. Heat Mass Transf. 125 (Oct. 2018) 994–1002, https://doi.org/10.1016/J.IJHEATMASSTRANSFER.2018.04.101.
[45] S. Mori, N. Maruoka, K. Okuyama, Critical heat flux enhancement by a two-layer structured honeycomb porous plate in a saturated pool boiling of water, Int. J. Heat Mass Transf. 118 (Mar. 2018) 429–438, https://doi.org/10.1016/J.IJHEATMASSTRANSFER.2017.10.100.
[46] S. Mori, S. Mt Aznam, and K. Okuyama, "Enhancement of the critical heat flux in saturated pool boiling of water by nanoparticle-coating and a honeycomb porous plate," *Int J Heat Mass Transf*, vol. 80, pp. 1–6, Jan. 2015, doi: 10.1016/J.IJHEATMASSTRANSFER.2014.08.046.
[47] M.R. Shattique, et al., Permeability of single-layer-free-standing meshes at varying capillary pressure via a novel method, Adv. Mater. Interfaces 10 (30) (Oct. 2023) 2300326, https://doi.org/10.1002/admi.202300326.
[48] Roman Giglio *et al.*, "Laser Processed Aluminum Nitride Structures for Enhanced Two-Phase Cooling," *SSRN*, 2024, [Online]. Available: https://papers.ssrn.com/sol3/papers.cfm?abstract_id=4808960.
[49] N. Fries, M. Dreyer, An analytic solution of capillary rise restrained by gravity, J. Colloid Interface Sci. 320 (1) (Apr. 2008) 259–263, https://doi.org/10.1016/J.JCIS.2008.01.009.
[50] P. Bowen, J. Highfield, A. Mocellin, Degradation of aluminum nitride powder in an aqueous environment, J. Am. Ceram. Soc. 73 (Mar. 1990) 724–728.
[51] R. Fitzpatrick, *Theoretical Fluid Mechanics*. Philadelphia: IOP Publishing, 2018.
[52] Z. Zhong, C. Huang, X. Wang, Enhanced pool boiling heat transfer of multilayer copper-nanoparticle-packed beds by copper mesh coating, Int. J. Therm. Sci. 184 (2023) 107965, https://doi.org/10.1016/j.ijthermalsci.2022.107965.
[53] M.M. Rahman, J. Pollack, M. McCarthy, Increasing boiling heat transfer using low conductivity materials, Sci. Rep. 5 (1) (2015) 13145, https://doi.org/10.1038/srep13145.
[54] G.S. Hwang, et al., Multi-artery heat-pipe spreader: Lateral liquid supply, Int. J. Heat Mass Transf. 54 (11–12) (2011) 2334–2340.
[55] A. Mukhopadhyay, A. Pal, S. Sarkar, and C. M. Megaridis, "Laser-Tuned Surface Wettability Modification and Incorporation of Aluminum Nitride (AlN) Ceramics in Thermal Management Devices," *Adv Funct Mater*, vol. 34, no. 18, May 2024, doi: 10.1002/adfm.202313141.
[56] C.M. Barnes, P.E. Tuma, Practical considerations relating to immersion cooling of power electronics in traction systems, IEEE Trans. Power Electron. 25 (9) (Sep. 2010) 2478–2485, https://doi.org/10.1109/TPEL.2010.2049864.
[57] A. Bar-Cohen, Thermal design of immersion cooling modules for electronic components, Heat Transf. Eng. 4 (3–4) (1983) 35–50, https://doi.org/10.1080/01457638108939607.